Self-interacting dark matter and muon $(g-2)$ in a gauged $U(1)_{L_\mu - L_\tau}$ model

Ayuki Kamada,[a] **Kunio Kaneta,**[a,b,c] **Keisuke Yanagi**[d] **and Hai-Bo Yu**[e]

[a]*Center for Theoretical Physics of the Universe, Institute for Basic Science (IBS),*
55 Expo-ro, Yuseong-gu, Daejeon 34126, Korea

[b]*School of Physics and Astronomy, University of Minnesota,*
116 Church Street S.E., Minneapolis, MN 55455, U.S.A.

[c]*William I. Fine Theoretical Physics Institute, University of Minnesota,*
116 Church Street S.E., Minneapolis, MN 55455, U.S.A.

[d]*Department of Physics, University of Tokyo,*
7-3-1, Hongo, Bunkyo-ku, Tokyo 113-0033, Japan

[e]*Department of Physics and Astronomy, University of California,*
900 University Avenue, Riverside, CA 92521, U.S.A.

E-mail: akamada@ibs.re.kr, kkaneta@umn.edu,
yanagi@hep-th.phys.s.u-tokyo.ac.jp, haiboyu@ucr.edu

ABSTRACT: We construct a self-interacting dark matter model that could simultaneously explain the observed muon anomalous magnetic moment. It is based on a gauged $U(1)_{L_\mu - L_\tau}$ extension of the standard model, where we introduce a vector-like pair of fermions as the dark matter candidate and a new Higgs boson to break the symmetry. The new gauge boson has a sizable contribution to muon $(g-2)$, while being consistent with other experimental constraints. The $U(1)_{L_\mu - L_\tau}$ Higgs boson acts as a light force carrier, mediating dark matter self-interactions with a velocity-dependent cross section. It is large enough in galaxies to thermalize the inner halo and explain the diverse rotation curves and diminishes towards galaxy clusters. Since the light mediator dominantly decays to the $U(1)_{L_\mu - L_\tau}$ gauge boson and neutrinos, the astrophysical and cosmological constraints are weak. We study the thermal evolution of the model in the early Universe and derive a lower bound on the gauge boson mass.

Contents

1 Introduction

Dark matter (DM) makes up 85% of the mass in the Universe, but its nature remains largely unknown. There has been great progress in studying particle DM candidates associated with extensions of the standard model (SM) of particle physics, which can be probed in high-energy and intensity-frontier terrestrial experiments (see, e.g., ref. [1]). Astrophysical and cosmological observations can also provide important clues to the nature of DM. In fact, a number of astrophysical observations indicate that the cold dark matter (CDM) model may break down on galactic scales (see refs. [2, 3] for a review), although it works remarkably well in explaining large-scale structure of the Universe, from Mpc to Gpc scales. For example, the galactic rotation curves of spiral galaxies exhibit a great diversity in inner shape [4], which is hard to understand in CDM. It has been shown that the diverse rotation curves can be explained naturally if DM has strong self-interactions [5, 6]. The analysis has been extended to the dwarf spheroidal galaxies in the Milky Way [7] and other galactic systems [8, 9]. This self-interacting dark matter (SIDM) scenario has rich implications for understanding the stellar kinematics of dwarf spheroidal galaxies and galaxy clusters and interpreting DM direct, indirect, and collider search results (see, e.g., ref. [2]).

On the particle physics side, there is also a long-standing puzzle that the measured muon anomalous magnetic moment, $(g-2)_\mu$, is larger than predicted in the SM at the 3σ level [10, 11]. This discrepancy may indicate that there is new physics beyond the SM

associated with the muon sector. In this work, we propose a model that could simultaneously explain the $(g-2)_\mu$ measurement and provide a realization of SIDM. It is based on a gauged $U(1)_{L_\mu-L_\tau}$ extension of the SM (see, e.g., refs. [12, 13]). Aside from the new gauge (Z') and Higgs (φ) bosons related to the symmetry, we introduce a vector-like pair of fermions (N and $\bar{N}$) as the DM candidate and assume that they couple to φ via a Yukawa interaction. The model overcomes a number of challenges in SIDM model building [14] (see also, e.g, refs. [15–28]). Our main observations are the following:

- The presence of Z' could contribute to $(g-2)_\mu$. If Z' has a mass in the range of $m_{Z'} \sim 10$–100 MeV, there is a viable parameter space to explain the $(g-2)_\mu$ anomaly.

- Astrophysical observations indicate that the DM self-scattering cross section per unit mass is $\sigma/m \gtrsim 1\,\mathrm{cm}^2/\mathrm{g}$ in galaxies, while diminishing to $\sigma/m \lesssim 0.1\,\mathrm{cm}^2/\mathrm{g}$ in galaxy clusters [8]. The desired velocity-dependence of σ/m can be achieved if $m_\varphi \sim 10$–100 MeV.

- In the early Universe, the mediator φ is in equilibrium with Z' and the SM neutrinos (ν_μ and ν_τ), and its number density is Boltzmann suppressed when the temperature is below its mass. Thus, the model avoids over-closing the Universe.

- Since Z' and φ dominantly decay to the neutrinos, the big bang nucleosynthesis (BBN), cosmic microwave background (CMB), and indirect detection bounds are significantly weaker, compared to the models with electrically charged final states [29, 30].

This paper is organized as follows. We introduce the $U(1)_{L_\mu-L_\tau}$ model and discuss relevant experimental and cosmological constraints in section 2. We discuss DM phenomenology of the model in section 3 and devote section 4 to conclusions. In the appendix, we provide detailed discussion on the neutrino-electron scattering cross section induced by Z' (A), the temperature evolution of the model in the early Universe (B), and the decay width of φ (C).

2 The model

We introduce a vector-like pair of fermions N and $\bar{N}$ and a $U(1)_{L_\mu-L_\tau}$ Higgs Φ in addition to the $U(1)_{L_\mu-L_\tau}$ gauge boson Z'_μ. The charge assignments are summarized in table 1.

The renormalizable Lagrangian density can be written as

$$\mathcal{L} = \mathcal{L}_{\mathrm{SM}} + g'Z'_\mu \left(L_2^\dagger \bar{\sigma}^\mu L_2 - L_3^\dagger \bar{\sigma}^\mu L_3 - \bar{\mu}^\dagger \bar{\sigma}^\mu \bar{\mu} + \bar{\tau}^\dagger \bar{\sigma}^\mu \bar{\tau} \right) - \frac{1}{4} Z'_{\mu\nu} Z'^{\mu\nu} - \frac{1}{2}\epsilon\, Z'_{\mu\nu} B^{\mu\nu}$$
$$+ (D_\mu \Phi)^\dagger D^\mu \Phi - V(\Phi, H) + iN^\dagger \bar{\sigma}^\mu D_\mu N + i\bar{N}^\dagger \bar{\sigma}^\mu D_\mu \bar{N}$$
$$- m_N N\bar{N} - \frac{1}{2} y_N \Phi NN - \frac{1}{2} y_{\bar{N}} \Phi^* \bar{N}\bar{N} + \mathrm{h.c.} \tag{2.1}$$

The covariant derivative on $U(1)_{L_\mu-L_\tau}$-charged particles is written as $D_\mu = \partial_\mu - ig'Q Z'_\mu$, where Q is a $U(1)_{L_\mu-L_\tau}$ charge. The field strengths of Z'_μ and the $U(1)_Y$ gauge boson B_μ

		SU(2)	U(1)$_Y$	U(1)$_{L_\mu - L_\tau}$
fermion	$L_2 = (\nu_\mu,\ \mu_L)$	2	$-1/2$	$+1$
	$L_3 = (\nu_\tau,\ \tau_L)$	2	$-1/2$	-1
	$\bar\mu = \mu_R^\dagger$	1	$+1$	-1
	$\bar\tau = \tau_R^\dagger$	1	$+1$	$+1$
	N	1	0	$1/2$
	$\bar N$	1	0	$-1/2$
scalar	H (SM Higgs)	2	$1/2$	0
	Φ	1	0	-1

Table 1. Charge assignments of the particles in the model, where the fermions are represented by the left-handed 2-component Weyl spinor.

are denoted by $Z'_{\mu\nu}$ and $B_{\mu\nu}$, respectively. The scalar potential of Φ takes a form of

$$V(\Phi, H) = -m_\Phi^2 |\Phi|^2 + \frac{1}{4}\lambda_\Phi |\Phi|^4 + \lambda_{\Phi H} |\Phi|^2 |H|^2. \tag{2.2}$$

We set $\lambda_{\Phi H} = 0$ so that it does not induce the DM interaction with SM particles through the Higgs portal. Φ develops a vacuum expectation value (VEV) and can be expanded as $\Phi(x) = (v_\Phi + \varphi(x))/\sqrt{2}$ in the unitary gauge, where $v_\Phi \simeq 2\sqrt{m_\Phi^2/\lambda_\Phi}$. The resultant masses of Z' and φ are given by $m_{Z'} = g' v_\Phi$ and $m_\varphi = \sqrt{\lambda_\Phi/2}\, v_\Phi$, respectively. Note that the VEV of Φ breaks U(1)$_{L_\mu - L_\tau}$ into a Z$_2$ symmetry, which stabilizes the lightest state of N and $\bar N$, i.e., the DM candidate. In our model, φ has a mass of $\mathcal{O}(10)\,$MeV and plays a role of the SIDM mediator.

We assume that there is no kinetic mixing between Z' and B at some high-energy scale, $\epsilon = 0$. This can be achieved by imposing a charge conjugation symmetry $C_{L_\mu - L_\tau}$: $L_2 \leftrightarrow L_3$, $\mu \leftrightarrow \tau$, $N \leftrightarrow \bar N$, $Z' \to -Z'$, and $\Phi \to \Phi^*$. However, since this symmetry is broken by the Yukawa mass terms of μ and τ, the mixings of Z' with the photon A and with the Z boson arise at the 1-loop level at low energy. The A-Z' mixing below m_μ is

$$\epsilon_{AZ'} = -\frac{eg'}{12\pi^2}\ln\left(\frac{m_\tau^2}{m_\mu^2}\right), \tag{2.3}$$

where e is the electric charge of the electron and m_μ and m_τ are the mu and tau lepton masses, respectively. To obtain the canonical gauge fields, we redefine the field as $A \to A + \epsilon_{AZ'}Z'$ for $|\epsilon_{AZ'}| \ll 1$. It induces a coupling between Z' and the SM electromagnetic current:

$$\mathcal{L}_{Z'\text{em}} = -\epsilon_{AZ'}e Z'_\mu J_\text{em}^\mu. \tag{2.4}$$

While the Z-Z' mixing is given by

$$\epsilon_{ZZ'} = \left(-\frac{1}{4} + s_W^2\right)\frac{eg'}{12\pi^2 s_W c_W}\ln\left(\frac{m_\tau^2}{m_\mu^2}\right), \tag{2.5}$$

where $c_W = \cos\theta_W$ and $s_W = \sin\theta_W$ with θ_W being the Weinberg angle. After performing the following field shifts: $Z \to Z - \epsilon_{ZZ'} r_{ZZ'}^2 Z'$ and $Z' \to Z' + \epsilon_{ZZ'} Z$, for $|\epsilon_{ZZ'}| \ll r_{ZZ'} \equiv m_{Z'}/m_Z \ll 1$, we have the coupling of Z to the $\mathrm{U}(1)_{L_\mu - L_\tau}$ current,

$$\mathcal{L}_{L_\mu - L_\tau Z} = -g' \epsilon_{ZZ'} Z_\mu J^\mu_{L_\mu - L_\tau}, \tag{2.6}$$

and the coupling of Z' to the SM neutral current,

$$\mathcal{L}_{Z'\mathrm{neu}} = \frac{e}{s_W c_W} \epsilon_{ZZ'} r_{ZZ'}^2 Z'_\mu J^\mu_{\mathrm{neu}}. \tag{2.7}$$

Since the coupling of Z' to the neutral current is suppressed by $m_{Z'}^2/m_Z^2 \sim 10^{-8}$, its contribution to Z' phenomenology is negligible. In the rest of this section, we discuss the observational constraints on Z' and φ.

2.1 Experimental constraints

The muon anomalous magnetic moment $a_\mu = (g-2)_\mu/2$ is measured in the Brookhaven E821 experiment [31, 32], and its value shows a 3σ deviation from the SM prediction. Depending on the uncertainty in the hadronic vacuum polarization contributions, the difference is evaluated as $a_\mu^{\mathrm{exp}} - a_\mu^{\mathrm{SM}} = (26.1 \pm 8.0) \times 10^{-10}$ [10] or $a_\mu^{\mathrm{exp}} - a_\mu^{\mathrm{SM}} = (28.7 \pm 8.0) \times 10^{-10}$ [11].[1] Through its interaction with the muon, Z' provides a sizable correction to $(g-2)_\mu$. The 1-loop contribution is evaluated as [35–37]

$$\Delta a_\mu^{Z'} = \frac{g'^2}{8\pi^2} \int_0^1 dx \frac{2m_\mu^2 x^2 (1-x)}{x^2 m_\mu^2 + (1-x) m_{Z'}^2}. \tag{2.8}$$

Since $\Delta a_\mu^{Z'} \simeq g'^2/(8\pi^2) = 32 \times 10^{-10} \left(g'/5 \times 10^{-4}\right)^2$ for $m_{Z'} \ll m_\mu$, the requirement of $\Delta a_\mu^{Z'} < a_\mu^{\mathrm{exp}} - a_\mu^{\mathrm{SM}}$ gives $g' \lesssim 5 \times 10^{-4}$. Thus, the upper limit, $g' \simeq 5 \times 10^{-4}$, is favored for resolving the discrepancy. In figure 1 (left), we show the favored parameter regions for the $(g-2)_\mu$ measurement, where we have used the result in ref. [10].

Figure 1 (left) also summarizes the current experimental constraints on the model, and we provide some details in the following:

- **Neutrino trident production.** The cross sections for $\nu N \to \nu N \mu\bar{\mu}$ at specific scattering energies have been measured in neutrino beam experiments, such as CHARM-II [39] and CCFR [40], and the results are in a good agreement with the SM predictions. We present the CCFR constraint on the model [41] in figure 1 (left).

- **Υ decays.** The BABAR experiment has searched for the $e\bar{e} \to \mu\bar{\mu} Z'$ process followed by $Z' \to \mu\bar{\mu}$ at the Υ resonance [42], resulting an upper limit on g' for $200\,\mathrm{MeV} \lesssim m_{Z'} \lesssim 10\,\mathrm{GeV}$.

---

[1]We adopt $\Delta a_\mu^{\mathrm{LbL}} = (10.5 \pm 2.6) \times 10^{-10}$ [33] as the hadronic light-by-light scattering contributions. Another group evaluates it as $\Delta a_\mu^{\mathrm{LbL}} = (11.6 \pm 4.0) \times 10^{-10}$ [34]. In any case, the discrepancy between the theoretical prediction and the experimental result is at the 3σ level.
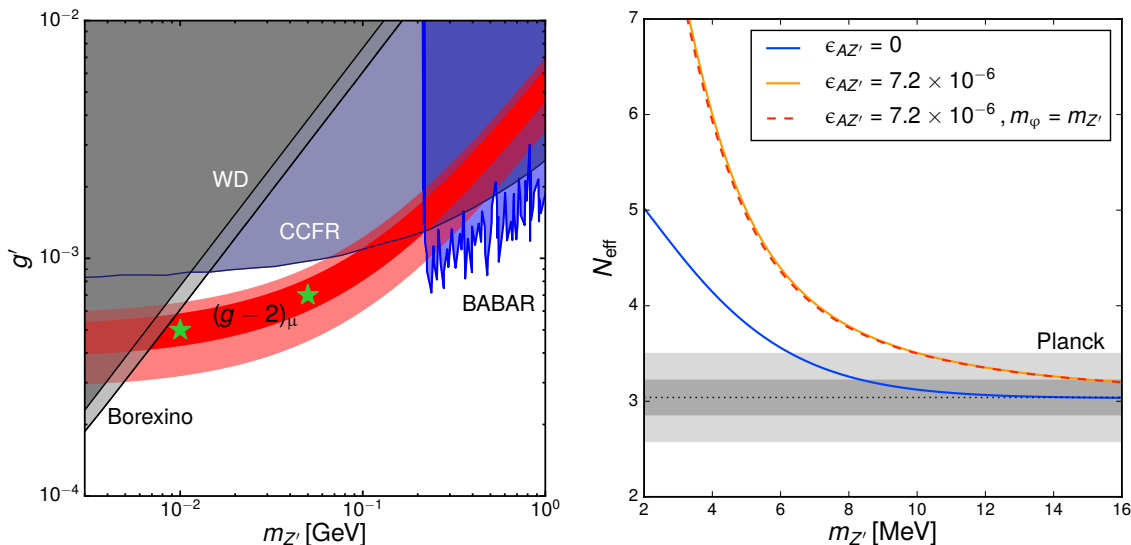
Figure 1. Left: parameter regions favored by the measurement of the muon anomalous magnetic moment within the 1σ (red) and 2σ (pink) limits, together with constraints (shaded) from various experiments, including BABAR (blue), CCFR (dark blue), Borexino (gray), and white dwarf cooling (dark gray). The green stars denote two examples shown in figure 2. Right: predicted effective neutrino degrees of freedom at the temperature below m_e, for different $\epsilon_{AZ'}$ values in the presence of only Z' (solid), and both Z' and φ (dashed). The gray shaded regions denote the results from the Planck collaboration (*Planck* TT, TE, EE+lowP+BAO) at the 1σ (dark) and 2σ (light) levels [38].

- **ν–e scattering.** The Borexino experiment measures the interaction rate of the mono-energetic $862\,\text{keV}$ ^{7}Be solar neutrino [43]. It puts a strong constraint on models that predict new ν-e interactions. In this work, we calculate the ν–e reaction rate by taking into account the Z' contribution (see appendix A for details). We require that the total reaction rate deviates from the SM prediction no more than 8% [43] and obtain the bound.

- **White dwarf (WD) cooling.** The white dwarf cooling also gives a strong limit [44]. The plasmon in the white dwarf star could decay to neutrinos through off-shell Z', and this process increases the cooling efficiency. In the SM, the effective operator $C_V G_F/\sqrt{2}\left[\bar{\nu}\gamma^\mu(1-\gamma^5)\nu\right]\left[\bar{e}\gamma_\mu e\right]$, where G_F is the Fermi constant and $C_V \simeq 0.964$ [45], induces the plasmon decay through the electron loop. In our model, we have a similar operator, $G_{Z'}\left[\bar{\nu}\gamma^\mu(1-\gamma^5)\nu\right]\left[\bar{e}\gamma_\mu e\right]$, where $G_{Z'} = -eg'\epsilon_{AZ'}/(2m_{Z'}^2)$. Demanding $G_{Z'} \lesssim C_V G_F$, we obtain $(g'/7.7 \times 10^{-4})^2(10\,\text{MeV}/m_{Z'})^2 \lesssim 1$, which is close to the Borexino bound.

It is remarkable that given these constraints there is still a viable parameter space for explaining $(g-2)_\mu$, i.e., $5\,\text{MeV} \lesssim m_{Z'} \lesssim 200\,\text{MeV}$ and $3.0 \times 10^{-4} \lesssim g' \lesssim 1.1 \times 10^{-3}$. Since Z' does not couple to the electron directly, our model is much less constrained when compared to others invoking a new gauge boson, such as the $U(1)_{B-L}$ model [46] and the hidden photon model with the kinetic mixing (see, e.g., ref. [47]). In what follows, we take

two model examples: $(m_{Z'}, g') = (10\,\text{MeV}, 5 \times 10^{-4})$ and $(50\,\text{MeV}, 7 \times 10^{-4})$ as indicated in figure 1 (green stars).

2.2 Cosmological constraint

The main decay channel of Z' is $Z' \to \nu\bar{\nu}$, and its lifetime is

$$\tau_{Z'} = 1 \times 10^{-14}\,\text{sec}\left(\frac{g'}{5 \times 10^{-4}}\right)^{-2}\left(\frac{m_{Z'}}{10\,\text{MeV}}\right)^{-1}. \qquad (2.9)$$

For the model parameters that we are interested in, $\tau_{Z'}$ is much shorter than the BBN timescale, $t \sim 1\,\text{sec}\,(1\,\text{MeV}/T)^2$. Thus, Z' is in equilibrium with ν_μ and ν_τ through the decay and inverse decay, after neutrinos decouple from the SM plasma, $T = T_{\nu\text{-dec}} \simeq 1.5\,\text{MeV}$. Its energy density is suppressed by the Boltzmann factor at $T \ll m_e, m_{Z'}$, and its direct contribution to the effective number of neutrino degrees of freedom N_{eff} is negligible. Note N_{eff} is related to the total energy density (ρ_{tot}) and the photon density (ρ_γ) as

$$\rho_{\text{tot}} = \rho_\gamma\left[1 + N_{\text{eff}}\frac{7}{8}\left(\frac{4}{11}\right)^{4/3}\right]. \qquad (2.10)$$

Even in this case, the presence of Z' may modify N_{eff}, since Z' injects energy only into ν_μ and ν_τ and it changes the ratio of the neutrino temperature to the photon temperature. In the limit of $\epsilon_{AZ'}=0$, we follow the analysis in ref. [48] to estimate the effect. We assume that (γ, e), (ν_e), and (ν_μ, ν_τ, Z') form independent thermal baths after the neutrino decoupling, and the comoving entropy density is conserved in each bath. By following the temperature evolution in each sector, we evaluate N_{eff} at $T \ll m_e, m_{Z'}$. In figure 1 (right), we show the lower bound on $m_{Z'}$ (blue), i.e., $m_{Z'} \gtrsim 6\,\text{MeV}$, where we take the upper limit $N_{\text{eff}} < 3.5$ [38].

In the presence of a sizable $\epsilon_{AZ'}$ as in eq. (2.3), Z' can decay to $e\bar{e}$, and there is heat transfer between (ν_μ, ν_τ, Z') and (γ, e) baths. In this case, we implement the heat transfer through $Z' \to e\bar{e}$ in the evolution of the comoving entropy density as

$$\frac{1}{a^3}\frac{d}{dt}[s_\gamma(T)a^3 + 2s_e(T)a^3] = \frac{1}{T}\Gamma_{Z' \to e\bar{e}}[\rho_{Z'}(T') - \rho_{Z'}(T)], \qquad (2.11)$$

$$\frac{1}{a^3}\frac{d}{dt}[2s_{\nu_\mu}(T')a^3 + 2s_{\nu_\tau}(T')a^3 + s_{Z'}(T')a^3] = -\frac{1}{T'}\Gamma_{Z' \to e\bar{e}}[\rho_{Z'}(T') - \rho_{Z'}(T)], \qquad (2.12)$$

$$\frac{1}{a^3}\frac{d}{dt}[2s_{\nu_e}(T_\nu)a^3] = 0, \qquad (2.13)$$

where T, T_ν, and T', denote the temperatures of (γ, e), (ν_e), and (ν_μ, ν_τ, Z'), respectively, and $\Gamma_{Z' \to e\bar{e}}$ is the decay width of $Z' \to e\bar{e}$,

$$\Gamma_{Z' \to e\bar{e}} = \frac{\alpha\epsilon_{AZ'}^2(m_{Z'}^2 + 2m_e^2)\sqrt{m_{Z'}^2 - 4m_e^2}}{3m_{Z'}^2}, \qquad (2.14)$$

where α is the fine-structure constant and m_e is the electron mass. Note that $\rho_{Z'}$ for the decay is evaluated with T', while $\rho_{Z'}$ for the inverse decay is evaluated with T. We

numerically solve eqs. (2.11)–(2.13) with the Hubble expansion rate,

$$H = \sqrt{\frac{\rho_\gamma(T) + 2\rho_e(T) + 2\rho_{\nu_e}(T_\nu) + 2\rho_{\nu_\mu}(T') + 2\rho_{\nu_\tau}(T') + \rho_{Z'}(T')}{3m_{\rm Pl}^2}},$$ (2.15)

where $m_{\rm Pl}$ is the reduced Planck mass. See appendix B for detailed discussion on the temperature evolution. We obtain $N_{\rm eff}$ as shown in figure 1 (right). For $N_{\rm eff} < 3.5$ and $\epsilon_{AZ'} \simeq 7.2 \times 10^{-6}$ (orange), corresponding to $g' = 5 \times 10^{-4}$, the lower bound is $m_{Z'} \gtrsim 10\,{\rm MeV}$ and stronger than the limit for $\epsilon_{AZ'} = 0$.

In this model, $\varphi\varphi \leftrightarrow Z'Z'$ and $\varphi\nu \leftrightarrow Z'\nu$ keep φ in equilibrium with Z' and thus with SM particles below $T \sim 20\,{\rm GeV}$ for $g' = 5 \times 10^{-4}$. To be conservative, we can assume that $m_\varphi > m_{Z'}$ so that the lifetime of φ is less than $1\,{\rm s}$ (see appendix C). In this case, the presence of φ does not change the lower bound on $m_{Z'}$ as shown in figure 1 (right). We comment on the possibility of $m_\varphi < m_{Z'}$, where φ decouples from the thermal bath when $\varphi\nu \leftrightarrow Z'\nu$ becomes inefficient. In this case, φ dominantly decays to four neutrinos long after the BBN. It can also decay to two neutrinos and two electrons with a small branching ratio $\sim e^2\epsilon_{AZ'}^2/g'^2$. The latter process could inject electromagnetic energy to the plasma and lead to observational consequences. If the φ lifetime is longer than $10^6\,{\rm s}$, the energy injection could distort the CMB spectrum from the blackbody radiation (see, e.g., ref. [49]). We find that m_φ has a lower limit, i.e., $m_\varphi \gtrsim 6\,{\rm MeV}$, to satisfy the COBE constraint [50] for $(m_{Z'}, g') = (10\,{\rm MeV}, 5 \times 10^{-4})$, while $m_\varphi \gtrsim 20\,{\rm MeV}$ for $(m_{Z'}, g') = (50\,{\rm MeV}, 7 \times 10^{-4})$. In addition, the observation of the light-element abundances can further tighten the constraint (see, e.g., ref. [51]). A detailed study of the cosmological constraint is beyond the scope of this work, and we will take the conservative assumption in the rest of the paper.

3 Dark Matter phenomenology

In this section, we discuss DM phenomenology predicted in this model. The mass matrix of the DM candidates N and $\bar{N}$ can be diagonalized by a unitary matrix U as

$$-\mathcal{L}_{\rm mass} = \frac{1}{2}\begin{pmatrix} N & \bar{N} \end{pmatrix}\begin{pmatrix} y_N\frac{v_\Phi}{\sqrt{2}} & m_N \\ m_N & y_{\bar{N}}\frac{v_\Phi}{\sqrt{2}} \end{pmatrix}\begin{pmatrix} N \\ \bar{N} \end{pmatrix} = \frac{1}{2}\begin{pmatrix} N_1 & N_2 \end{pmatrix}\begin{pmatrix} M_1 & 0 \\ 0 & M_2 \end{pmatrix}\begin{pmatrix} N_1 \\ N_2 \end{pmatrix},$$ (3.1)

where $0 \le M_1 \le M_2$ and

$$\begin{pmatrix} N_1 \\ N_2 \end{pmatrix} = U\begin{pmatrix} N \\ \bar{N} \end{pmatrix}.$$ (3.2)

Then the Lagrangian density in the 4-component spinor notation, where N_i denotes a Majorana fermion, becomes

$$\mathcal{L} \supset \frac{i}{2}\overline{N}_i\gamma^\mu\partial_\mu N_i - \frac{1}{2}M_i\overline{N}_i N_i + \frac{g'}{4}Z'_\mu\overline{N}_i\left[i{\rm Im}(U_{i1}U_{j1}^* - U_{i2}U_{j2}^*) + {\rm Re}(U_{i1}U_{j1}^* - U_{i2}U_{j2}^*)\gamma_5\right]\gamma^\mu N_j$$

$$- \frac{1}{2\sqrt{2}}\varphi\overline{N}_i\left[{\rm Re}(y_N U_{i1}^* U_{j1}^* + y_{\bar{N}}U_{i2}^* U_{j2}^*) - i{\rm Im}(y_N U_{i1}^* U_{j1}^* + y_{\bar{N}}U_{i2}^* U_{j2}^*)\gamma_5\right]N_j.$$ (3.3)

We consider two extreme cases to illustrate the main predictions of our model and further simplify the Lagrangian density.

- **Pseudo-Majorana DM**, where $|y_{\bar{N}}|v_\Phi > |y_N|v_\Phi \gg |m_N|$. After performing the phase rotation of N and $\bar{N}$ such that both y_N and $y_{\bar{N}}$ are positive, we have $M_1 \approx y_N v_\Phi/\sqrt{2}$ and $M_2 \approx y_{\bar{N}} v_\Phi/\sqrt{2}$. Note that DM phenomenology is unchanged for $|y_N|v_\Phi > |y_{\bar{N}}|v_\Phi \gg |m_N|$. In this limit, it turns out that we cannot simultaneously obtain the SIDM cross section, explain the $(g-2)_\mu$ discrepancy, and realize viable cosmology. We will not focus on this case in the rest of the paper.

- **Pseudo-Dirac DM**, where $|m_N| \gg |y_N|v_\Phi, |y_{\bar{N}}|v_\Phi$. We choose a basis such that m_N and $y_N^* + y_{\bar{N}}$ are positive and further restrict our discussion to the case where $y_N = y_{\bar{N}} \equiv y > 0$. In this limit, the DM sector respects $C_{L_\mu - L_\tau}$ ($N \leftrightarrow \bar{N}$ and $\Phi \to \Phi^*$) and the parity conjugation ($N \to i\bar{N}^\dagger$ and $\bar{N} \to iN^\dagger$). The mass eigenstates are $N_1 = (N - \bar{N})/(\sqrt{2}i)$ and $N_2 = (N + \bar{N})/\sqrt{2}$, and the corresponding masses are $M_1 \approx m_N - yv_\Phi/\sqrt{2}$ and $M_2 \approx m_N + yv_\Phi/\sqrt{2}$. The gauge and Yukawa interactions are

$$\mathcal{L} \supset -\frac{y}{2\sqrt{2}}\varphi\left(-\overline{N}_1 N_1 + \overline{N}_2 N_2\right) + ig'Q_N Z'_\mu \overline{N}_2 \gamma^\mu N_1 \,. \tag{3.4}$$

To explore DM phenomenology predicted in this pseudo-Dirac case, we need to specify five parameters: $m_{Z'}$, g', m_φ, M_1, and y. For the first two, we take the examples motivated by the $(g-2)_\mu$ measurement as denoted by the green stars in figure 1 (left). We then scan the (m_φ, M_1) parameter space, while fixing y by the relic density requirement accordingly, as discussed next.

3.1 DM relic abundance

We determine the Yukawa coupling y such that the N_1 relic density gives rise to the observed DM abundance. We assume that $M_1 \sim M_2 \lesssim 100\,\text{GeV}$ so that the freeze-out occurs after the $U(1)_{L_\mu - L_\tau}$ symmetry breaking, $T < v_\Phi = \mathcal{O}(10)\,\text{GeV}$, and we can neglect the thermal corrections to $\Delta M = M_2 - M_1 = \sqrt{2}yv_\Phi$, m_φ, and $m_{Z'}$.[2] Since $\Delta M = \mathcal{O}(1)\,\text{GeV}$, N_1 and N_2 are in equilibrium with each other during the freeze-out and we need to take into account their co-annihilation process [52]. The annihilation channels are $N_1 N_1, N_2 N_2 \to Z'Z', \varphi\varphi$ and $N_1 N_2 \to \varphi Z'$, and the corresponding thermally-averaged cross sections times relative velocity can be written as

$$\langle \sigma_{\text{ann}} v_{\text{rel}} \rangle_{11} = \langle \sigma_{\text{ann}} v_{\text{rel}} \rangle_{22} \simeq \frac{9y^4}{64\pi m_N^2} x^{-1}, \quad \langle \sigma_{\text{ann}} v_{\text{rel}} \rangle_{12} \simeq \frac{y^4}{64\pi m_N^2} - \frac{9y^4}{256\pi m_N^2} x^{-1}, \tag{3.5}$$

where $x = M_1/T$. In deriving eq. (3.5), we have ignored the terms depending on g', since they are too small to play a role. The effective annihilation cross section is

$$\langle \sigma_{\text{ann}} v_{\text{rel}} \rangle_{\text{eff}} = \langle \sigma_{\text{ann}} v_{\text{rel}} \rangle_{11} r_1^2 + \langle \sigma_{\text{ann}} v_{\text{rel}} \rangle_{22} r_2^2 + 2\langle \sigma_{\text{ann}} v_{\text{rel}} \rangle_{12} r_1 r_2, \tag{3.6}$$

---

[2]This mass range is also compatible with the naturalness requirement of λ_Φ. The sizable DM self-scattering cross section requires $m_\varphi \sim 10\,\text{MeV}$, which corresponds to $\lambda_\Phi \sim 10^{-6}$ for $v_\Phi \sim 10\,\text{GeV}$. The dominant correction to λ_Φ comes from the fermion box diagrams and is estimated as $y^4/(16\pi^2)$. For $y \sim 10^{-2}$–10^{-1}, as determined by the relic density consideration, the correction to λ_Φ is less than a factor of 10^{-6} for $m_N \lesssim 100\,\text{GeV}$.

where $r_1 = 1/(1 + e^{-\Delta x})$, $r_2 = e^{-\Delta x}/(1 + e^{-\Delta x})$, and $\Delta \equiv \Delta M/m_N$. We equate this effective annihilation cross section to the canonical one, $\langle \sigma_{\text{ann}} v_{\text{rel}} \rangle_{\text{can}} = 3 \times 10^{-26} \, \text{cm}^3/\text{s}$, at $x_f = 20$ and derive the y value for given (m_φ, M_1). We have checked that the Sommerfeld effect is negligible for the freeze-out calculation (see, e.g., refs. [53, 54]) for the DM mass range that we are interested in.

3.2 DM self-scattering

The elastic scattering of N_1 is dominated by the Yukawa interaction in eq. (3.4), which is represented by the following Yukawa potential for non-relativistic scattering:

$$V(r) = -\frac{y^2}{4\pi r} e^{-m_\varphi r}, \tag{3.7}$$

where the y value is fixed by the relic density consideration as discussed above. The scattering amplitude $f(\theta)$ is given by the partial wave expansion as

$$f(\theta) = \frac{2}{M_1 v_{\text{rel}}} \sum_{\ell=0}^{\infty} (2\ell + 1) e^{i\delta_\ell} \sin \delta_\ell P_\ell(\cos \theta), \tag{3.8}$$

where δ_ℓ is the phase shift and P_ℓ is the ℓth order Legendre polynomial. We numerically calculate δ_ℓ by solving the Schrödinger equation as in ref. [55]. Since N_1 is a Majorana fermion, the scattering particles are indistinguishable. Then the differential cross section is given by the sum of spin-singlet and spin-triplet channel amplitudes as

$$\frac{d\sigma}{d\Omega} = \frac{1}{2} \times \left[\frac{1}{4} |f(\theta) + f(\pi - \theta)|^2 + \frac{3}{4} |f(\theta) - f(\pi - \theta)|^2 \right], \tag{3.9}$$

where the initial state is assumed to be unpolarized [56].

The standard cross section, $\sigma = \int d\Omega \, (d\sigma/d\Omega)$, is not an appropriate quantity for characterizing the effect of self-scattering on the structure formation, since the scattering through a light mediator receives strong enhancement at $\theta = 0$ and π, which do not affect the DM distribution. Instead the transfer cross section is often used in the literature [2], which is written for the scattering of identical particles as [57]

$$\sigma_T = 4\pi \int_0^1 d\cos\theta \, (1 - \cos\theta) \frac{d\sigma}{d\Omega}. \tag{3.10}$$

In figure 2, we show the parameter regions for $\sigma_T/M_1 = 0.1$–$1 \, \text{cm}^2/\text{g}$ (light blue) and 1–$10 \, \text{cm}^2/\text{g}$ (blue) in dwarf galaxies, 0.1–$1 \, \text{cm}^2/\text{g}$ (red) in Milky Way-size galaxies, and $> 0.1 \, \text{cm}^2/\text{g}$ (green) in galaxy clusters, where we take $v_{\text{rel}} = 30$, 200, and $1000 \, \text{km/s}$, respectively. We have used the Born approximation when it is valid. We see that with a light mediator, i.e., $m_\varphi = \mathcal{O}(10) \, \text{MeV}$, the SIDM cross section can be large in galaxies, while diminishing towards galaxy clusters, as shown in both panels. However, when we impose the cosmological constraint (gray), i.e., $m_\varphi > m_{Z'}$, most of the SIDM parameter space is excluded for the case of $g' = 7 \times 10^{-4}$ and $m_{Z'} = 50 \, \text{MeV}$ (right).

Figure 3 shows the velocity-dependence of the self-scattering cross section $\langle \sigma_T v_{\text{rel}} \rangle / M_1$, averaged over the Maxwell-Boltzmann distribution, for the three benchmark cases marked
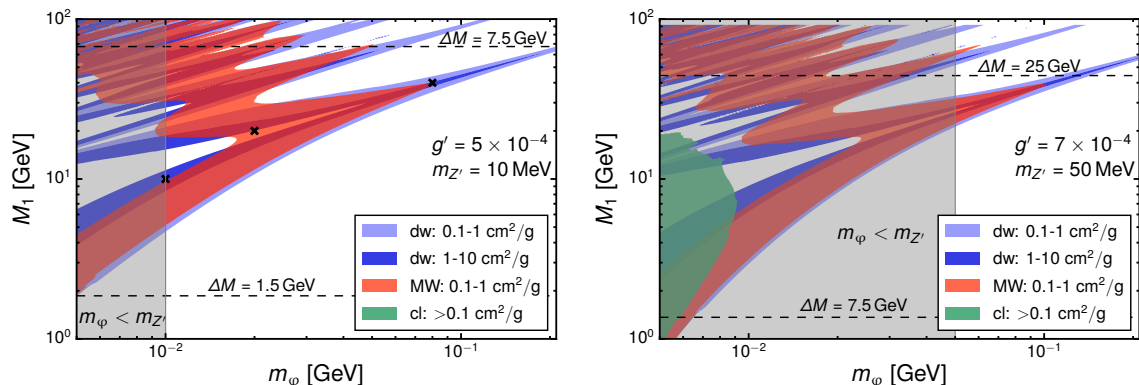
Figure 2. SIDM parameter regions for dwarf galaxies (blue), Milky Way-size galaxies (red), and galaxy cluster (green). We take $(m_{Z'}, g') = (10\,\mathrm{MeV}, 5 \times 10^{-4})$ (left) and $(50\,\mathrm{MeV}, 7 \times 10^{-4})$ (right). In the left panel, the self-scattering cross section is less than $0.1\,\mathrm{cm}^2/\mathrm{g}$ in galaxy clusters. The BBN observations disfavor $m_\varphi < m_{Z'}$ (gray). The dashed lines indicate the mass splittings between N_1 and N_2 states. The crosses (left) denote the benchmark cases shown in figure 3.
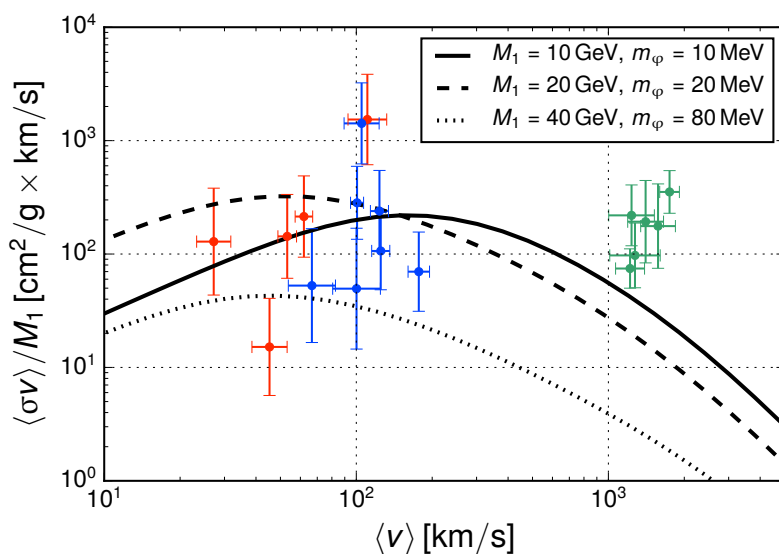
Figure 3. Self-interaction cross sections, $\langle \sigma_T v \rangle / M_1$, at the benchmark points taken from the left panel of figure 2. We take $(M_1, m_\varphi) = (10\,\mathrm{GeV}, 10\,\mathrm{MeV})$ (solid), $(20\,\mathrm{GeV}, 20\,\mathrm{MeV})$ (dashed) and $(40\,\mathrm{GeV}, 80\,\mathrm{MeV})$ (dotted). The points with errors are taken from ref. [8], corresponding to dwarf galaxies (red), low surface brightness galaxies (blue), and galaxy clusters (green).

in figure 2 (left), together with the inferred values from stellar kinematics of dwarf (red) and low surface brightness (blue) galaxies, and galaxy clusters (green) [8]. We see that at least two cases (solid and dashed) have a large self-scattering cross section to address the diversity problem of galactic rotation curves. On cluster scales, all three cases have a cross section below $\sim 0.1 \text{ cm}^2/\text{g}$, as required by the cluster constraints [8]. Interestingly, this upper limit is preferred if the DM self-interactions also explain the inferred density cores in the galaxy clusters [58]. The case with $M_1 = 10 \text{ GeV}$ may explain observations of stellar kinematics in both galaxies and galaxy clusters.

As indicated in figure 2, all three benchmark cases are in the resonance regime, where the self-scattering cross section has a strong velocity dependence [59], i.e., $\sigma_T/M_1 \propto 1/v_{\text{rel}}^2$. Thus, the cross sections decrease from $\gtrsim 1 \text{ cm}^2/\text{g}$ in dwarf galaxies to $< 0.1 \text{ cm}^2/\text{g}$ in galaxy clusters. This is a generic feature of the model due to the tight constraints. Combining the muon $(g-2)$ and the Borexino constraints, we require $m_{Z'} \gtrsim 10 \text{ MeV}$. We further demand $m_{\varphi} \gtrsim m_{Z'}$ so that φ decays before the onset of the BBN, and the Yukawa coupling constant y to be fixed by the DM relic abundance. After imposing all these constraints, we find that our SIDM model is in the resonant regime.

3.3 Direct and indirect searches

If the SIDM mediator decays through the Higgs portal, DM direct detection experiments have put a strong constraint on the mixing parameter $\lambda_{\Phi H}$ [14, 56, 60] and the lifetime of the mediator is too long to be consistent with early Universe cosmology. In the model we consider, φ decays to Z' to avoid over-closing the Universe. Thus, it does not need to mix with the SM Higgs boson to deplete its abundance. We set $\lambda_{\Phi H} = 0$ at the tree level. A finite value of $\lambda_{\Phi H}$ can be generated through a 2-loop process, but it is small and much below the experimental sensitivity. Moreover, the spin-dependent DM-nucleon scattering is inelastic, since the relevant interaction term involves two states, as shown in eq. (3.4). In this model, the predicted mass splitting is $\Delta M > 1 \text{ GeV}$ (see figure 2) which is much larger than the nuclei recoil energy in DM direct detection. Thus, DM direct searches do not constrain this model.

For indirect detection, the annihilation processes, $N_1 N_1 \to Z' Z'$ and $\varphi\varphi$, are p-wave dominated, and their final states decay to the SM neutrinos. Since the upper bound on the DM annihilation cross section to the neutrinos is $\langle \sigma_{\text{ann}} v_{\text{rel}} \rangle \lesssim 10^{-24} \text{ cm}^3/\text{s}$ [61], our model easily avoids the indirect detection constraints.

Before closing this section, we comment on the scenario where $y_N \neq y_{\bar{N}}$. In this case, there is a pseudo-scalar interaction, $i\varphi N_1 \gamma_5 N_1$, in addition to the scalar one. This new term induces a DM-DM potential that is suppressed by a factor of $m_{\varphi}^2/m_{N_1}^2$, compared to the Yukawa one. But, it is strongly singular as $V(r) \propto 1/r^3$. We expect it has a subdominant effect on DM self-interactions since in the Born approximation limit the pseudo-scalar cross section vanishes for $v_{\text{rel}} \to 0$. For the gauge interactions, we now need to include the DM axial current, $-(g'\kappa/2)Z'_{\mu}\overline{N}_1 \gamma_5 \gamma^{\mu} N_1$, with $\kappa \sim y v_{\Phi}/m_N$. It induces a DM-nucleon scattering cross section that decreases for $v_{\text{rel}} \to 0$. The current constraint, e.g., from the LUX experiment [62] is satisfied if $|\kappa| < \mathcal{O}(10^2)$ for $g' = 5 \times 10^{-4}$ with the momentum transfer $\sim 100 \text{ MeV}$ [63].

4 Conclusion

We have constructed a U(1)$_{L_\mu - L_\tau}$ model that could explain the $(g-2)_\mu$ measurement and reconcile the discrepancies of CDM on galactic scales. In this model, the U(1)$_{L_\mu - L_\tau}$ Higgs boson acts as the light dark force carrier, mediating DM self-interactions. We thoroughly studied the constraints from the high-energy and intensity-frontier experiments and cosmological and astrophysical observations, and found a viable model parameter space. Since the mediator dominantly decays to the neutrinos, the model avoids tight constraints from DM indirect searches. To be consistent with the cosmological upper bound, $N_{\text{eff}} < 3.5$, we found that the mediator φ and gauge boson Z' masses satisfy the condition of $m_\varphi > m_{Z'} \gtrsim$ 10 MeV. Interestingly, with the same mass range of Z', the model could also explain the dip feature [64, 65] in the IceCube neutrino spectrum [48, 66, 67]. Since the Higgs mixing term vanishes, our model does not lead to direct detection signals via the Higgs portal. In addition, our model naturally predicts a GeV mass splitting between two DM mass states, which forbids DM-nucleon scattering via the gauge boson-photon kinetic mixing.

Our model could be tested in future collider experiments, such as the facilities in the intensity frontier [68–72]. In addition, the observation of a nearby supernova may also provide important hints on the properties of Z', since the non-standard neutrino self-interaction shortens the mean free path and increases the neutrino diffusion time from the supernova core [48]. On the model building aspect, we could introduce three right-handed neutrinos and realize the see-saw mechanism to reproduce the observed neutrino masses and mixings [73].

A Neutrino-electron scattering rate

We provide details on the constraint from the neutrino-electron scattering discussed in section 2.1 (see also, e.g., refs. [74, 75]). The electron-neutrino scattering cross sections are

$$\frac{d\sigma_{\text{SM}}(\nu_e e)}{dT} = \frac{G_F^2 m_e}{2\pi}\left[\{(1+g_V)\pm(1+g_A)\}^2 + \{(1+g_V)\mp(1+g_A)\}^2\left(1-\frac{T}{E_\nu}\right)^2\right.$$
$$\left. -(g_V-g_A)(g_V+g_A+2)\frac{m_e T}{E_\nu^2}\right], \tag{A.1}$$

$$\frac{d\sigma_{\text{SM}}(\nu_\alpha e)}{dT} = \frac{G_F^2 m_e}{2\pi}\left[\{(g_V\pm g_A)+(g_V\mp g_A)\}^2\times\left(1-\frac{T}{E_\nu}\right)^2 - (g_V^2-g_A^2)\frac{m_e T}{E_\nu^2}\right], \tag{A.2}$$

$$\frac{d\sigma_{Z'}(\nu_\alpha e)}{dT} = \frac{g'^2(e\epsilon_{AZ'})^2 m_e}{4\pi(2m_e T + m_{Z'}^2)^2}\left[1 + \left(1 - \frac{T}{E_\nu}\right)^2 - \frac{m_e T}{E_\nu^2}\right]$$
$$+ \frac{g'e\epsilon_{AZ'}G_F m_e}{\sqrt{2}\pi(2m_e T + m_{Z'}^2)}\left[(g_V + g_A) + (g_V - g_A)\left(1 - \frac{T}{E_\nu}\right)^2 - g_V \frac{m_e T}{E_\nu^2}\right], \quad \text{(A.3)}$$

where $g_V = -1/2 + 2s_W^2$ and $g_A = -1/2$. The upper (lower) sign corresponds to the neutrino (anti-neutrino) and $\alpha = \mu, \tau$. The incident neutrino energy is $E_\nu = 862\,\text{keV}$ for the ^{7}Be solar neutrino. T is the electron recoil energy and its maximal value is $T_{\max} = 2E_\nu^2/(m_e + 2E_\nu)$. The minimal value of T is $T_{\min} \simeq 270\,\text{keV}$ for the Borexino experiment [43, 74]. Then, the total reaction rate R_{tot} is given by

$$\frac{dR_{\text{tot}}}{dT} = t_{\exp}\,\rho_e \int dE_\nu \frac{d\sigma_{\text{tot}}}{dT}\frac{d\Phi_{\nu_e}}{dE_\nu}, \quad \text{(A.4)}$$

where $t_{\exp}$ and ρ_e are the exposure time and the electron number density of the target, respectively. We assume that the neutrino spectrum $d\Phi_{\nu_e}/dE_\nu$ is mono-energetic at $E_\nu = 862\,\text{keV}$. Since we are only interested in the ratio between the total reaction rates with and without Z', the overall normalization is irrelevant for our discussion. We define the total cross section used in eq. (A.4) as

$$\sigma_{\text{tot}}(\nu e) = P_{ee}\,\sigma_{\text{SM}}(\nu_e e) + (1 - P_{ee})\sum_\alpha \left[\sigma_{\text{SM}}(\nu_\alpha e) + \sigma_{Z'}(\nu_\alpha e)\right], \quad \text{(A.5)}$$

with the electron neutrino survival probability $P_{ee} \simeq 0.51$ [43]. For the SM prediction, one drops the $\sigma_{Z'}$ contribution.

B   Temperature evolution around the BBN

We summarize the basic thermal quantities and show how the temperatures evolve around the BBN. The thermal distribution of particle a takes a form of

$$f_a(p,T) = \frac{1}{e^{\sqrt{p^2 + m_a^2}/T} \mp 1}, \quad \text{(B.1)}$$

where $-$ $(+)$ is taken when particle a is boson (fermion). The entropy and energy densities of particle a are given by

$$s_a(T) = g_a \int_0^\infty \frac{4\pi p^2 dp}{(2\pi)^3}\left[\frac{\sqrt{p^2 + m_a^2}}{T} + \frac{p^2}{3T\sqrt{p^2 + m_a^2}}\right]f_a(p,T), \quad \text{(B.2)}$$

$$\rho_a(T) = g_a \int_0^\infty \frac{4\pi p^2 dp}{(2\pi)^3}\sqrt{p^2 + m_a^2}\,f_a(p,T), \quad \text{(B.3)}$$

respectively, where g_a is the spin degrees of freedom of particle a. When $m_a \ll T$, the above integrations can be done analytically and read as

$$s_a(T) = g_a\left(\times\frac{7}{8}\right)\frac{2\pi^2}{45}T^3, \quad \text{(B.4)}$$

$$\rho_a(T) = g_a\left(\times\frac{7}{8}\right)\frac{\pi^2}{30}T^4, \quad \text{(B.5)}$$

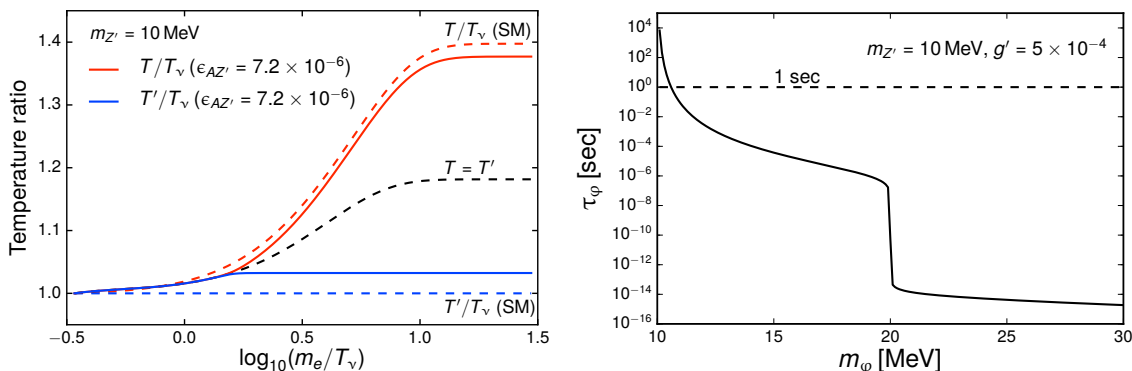where the factor of 7/8 is taken when particle a is fermion.

Figure 4. Left: evolution of T/T_ν (red) and T'/T_ν (blue) for $\epsilon_{AZ'} = 7.2 \times 10^{-6}$ (solid) and 0 (dashed). Shown also is the case for the tightly coupled limit, i.e., $T = T'$ (black dashed). Right: lifetime of φ as a function of m_φ.

In section 2.2, we introduced three temperatures: T is the temperature of (γ, e), T_ν is that of (ν_e), and T' is that of (ν_μ, ν_τ, Z'). We follow eqs. (2.11)–(2.13) and eq. (2.15). In figure 4 (left), we show the evolution of T/T_ν (red) and T'/T_ν (blue) for $\epsilon_{AZ'} = 7.2 \times 10^{-6}$ (solid) and the SM (dashed), together with the case where $(\gamma, e, \nu_\mu, \nu_\tau, Z')$ forms one thermal bath and thus $T = T'$ (black dashed). Note that T_ν is not affected by the presence of Z'. We see that $Z' \to e\bar{e}$ lowers T, while raises T', when compared to the case of the SM. This is because heat from $e\bar{e}$ annihilation is partially transferred from (γ, e) to (ν_μ, ν_τ, Z').

C Decay width of φ

For $m_\varphi \geq 2m_{Z'}$, the dominant decay channel is $\varphi \to Z'Z'$ and the decay width is

$$\Gamma_{\varphi \to Z'Z'} = \frac{g'^2 Q_\Phi^2}{32\pi} \frac{\sqrt{m_\varphi^2 - 4m_{Z'}^2}(m_\varphi^4 - 4m_\varphi^2 m_{Z'}^2 + 12m_{Z'}^4)}{m_\varphi^2 m_{Z'}^2} . \tag{C.1}$$

While for $m_{Z'} \leq m_\varphi < 2m_{Z'}$, the 3-body decay process, i.e., $\varphi \to Z'\nu\bar{\nu}$, dominates and the width is given by

$$\Gamma_{\varphi \to Z'\nu\bar{\nu}} = \frac{g'^4 Q_\Phi^2 m_{Z'}^4}{32\pi^3 m_\varphi^3} F\left(\frac{m_\varphi}{m_{Z'}}\right) , \tag{C.2}$$

where

$$F(r) = \int_0^{(r-1)^2} dx \int_{y_{\min}}^{y_{\max}} dy \frac{r^2(y-1) - x(y-2) - y(y-1)}{(x-1)^2 + w^2} , \tag{C.3}$$

$$y_{\max} = \frac{r^2 + \sqrt{r^4 - 2r^2(x+1) + (x-1)^2} - x + 1}{2} , \tag{C.4}$$

$$y_{\min} = \frac{r^2 - \sqrt{r^4 - 2r^2(x+1) + (x-1)^2} - x + 1}{2} , \tag{C.5}$$

In figure 4 (right), we show the lifetime of φ vs its mass. For $m_\varphi > m_{Z'}$, τ_φ is less than 1 s.

References

[1] M. Battaglieri et al., *U.S. cosmic visions — new ideas in dark matter* 2017*: community report*, [arXiv:1707.04591](https://arxiv.org/abs/1707.04591) [INSPIRE].

[2] S. Tulin and H.-B. Yu, *Dark matter self-interactions and small scale structure*, [*Phys. Rept.* **730** (2018) 1](https://doi.org/10.1016/j.physrep.2017.11.004) [arXiv:1705.02358](https://arxiv.org/abs/1705.02358) [INSPIRE].

[3] J.S. Bullock and M. Boylan-Kolchin, *Small-scale challenges to the ΛCDM paradigm*, [*Ann. Rev. Astron. Astrophys.* **55** (2017) 343](https://doi.org/10.1146/annurev-astro-091916-055313) [arXiv:1707.04256](https://arxiv.org/abs/1707.04256) [INSPIRE].

[4] K.A. Oman et al., *The unexpected diversity of dwarf galaxy rotation curves*, [*Mon. Not. Roy. Astron. Soc.* **452** (2015) 3650](https://doi.org/10.1093/mnras/stv1504) [arXiv:1504.01437](https://arxiv.org/abs/1504.01437) [INSPIRE].

[5] A. Kamada, M. Kaplinghat, A.B. Pace and H.-B. Yu, *Self-interacting dark matter can explain diverse galactic rotation curves*, [*Phys. Rev. Lett.* **119** (2017) 111102](https://doi.org/10.1103/PhysRevLett.119.111102) [arXiv:1611.02716](https://arxiv.org/abs/1611.02716) [INSPIRE].

[6] P. Creasey, O. Sameie, L.V. Sales, H.-B. Yu, M. Vogelsberger and J. Zavala, *Spreading out and staying sharp — creating diverse rotation curves via baryonic and self-interaction effects*, [*Mon. Not. Roy. Astron. Soc.* **468** (2017) 2283](https://doi.org/10.1093/mnras/stx522) [arXiv:1612.03903](https://arxiv.org/abs/1612.03903) [INSPIRE].

[7] M. Valli and H.-B. Yu, *Dark matter self-interactions from the internal dynamics of dwarf spheroidals*, [arXiv:1711.03502](https://arxiv.org/abs/1711.03502) [INSPIRE].

[8] M. Kaplinghat, S. Tulin and H.-B. Yu, *Dark matter halos as particle colliders: unified solution to small-scale structure puzzles from dwarfs to clusters*, [*Phys. Rev. Lett.* **116** (2016) 041302](https://doi.org/10.1103/PhysRevLett.116.041302) [arXiv:1508.03339](https://arxiv.org/abs/1508.03339) [INSPIRE].

[9] K. Bondarenko, A. Boyarsky, T. Bringmann and A. Sokolenko, *Constraining self-interacting dark matter with scaling laws of observed halo surface densities*, [*JCAP* **04** (2018) 049](https://doi.org/10.1088/1475-7516/2018/04/049) [arXiv:1712.06602](https://arxiv.org/abs/1712.06602) [INSPIRE].

[10] K. Hagiwara, R. Liao, A.D. Martin, D. Nomura and T. Teubner, $(g-2)_\mu$ *and* $\alpha(M_Z^2)$ *re-evaluated using new precise data*, [*J. Phys.* **G 38** (2011) 085003](https://doi.org/10.1088/0954-3899/38/8/085003) [arXiv:1105.3149](https://arxiv.org/abs/1105.3149) [INSPIRE].

[11] M. Davier, A. Hoecker, B. Malaescu and Z. Zhang, *Reevaluation of the hadronic contributions to the muon* $g-2$ *and to* $\alpha(M_Z^2)$, [*Eur. Phys. J.* **C 71** (2011) 1515](https://doi.org/10.1140/epjc/s10052-010-1515-z) [*Erratum ibid.* **C 72** (2012) 1874] [arXiv:1010.4180](https://arxiv.org/abs/1010.4180) [INSPIRE].

[12] X.-G. He, G.C. Joshi, H. Lew and R.R. Volkas, *Simplest Z′ model*, [*Phys. Rev.* **D 44** (1991) 2118](https://doi.org/10.1103/PhysRevD.44.2118) [INSPIRE].

[13] X.-G. He, G.C. Joshi, H. Lew and R.R. Volkas, *New Z′ phenomenology*, [*Phys. Rev.* **D 43** (1991) 22](https://doi.org/10.1103/PhysRevD.43.R22) [INSPIRE].

[14] M. Kaplinghat, S. Tulin and H.-B. Yu, *Direct detection portals for self-interacting dark matter*, [*Phys. Rev.* **D 89** (2014) 035009](https://doi.org/10.1103/PhysRevD.89.035009) [arXiv:1310.7945](https://arxiv.org/abs/1310.7945) [INSPIRE].

[15] F.-Y. Cyr-Racine and K. Sigurdson, *Cosmology of atomic dark matter*, [*Phys. Rev.* **D 87** (2013) 103515](https://doi.org/10.1103/PhysRevD.87.103515) [arXiv:1209.5752](https://arxiv.org/abs/1209.5752) [INSPIRE].

[16] J.M. Cline, Z. Liu, G.D. Moore and W. Xue, *Scattering properties of dark atoms and molecules*, *Phys. Rev.* **D 89** (2014) 043514 [arXiv:1311.6468] [ɪɴSPIRE].

[17] K.K. Boddy, J.L. Feng, M. Kaplinghat and T.M.P. Tait, *Self-interacting dark matter from a non-Abelian hidden sector*, *Phys. Rev.* **D 89** (2014) 115017 [arXiv:1402.3629] [ɪɴSPIRE].

[18] K.K. Boddy, J.L. Feng, M. Kaplinghat, Y. Shadmi and T.M.P. Tait, *Strongly interacting dark matter: self-interactions and keV lines*, *Phys. Rev.* **D 90** (2014) 095016 [arXiv:1408.6532] [ɪɴSPIRE].

[19] N. Bernal, X. Chu, C. Garcia-Cely, T. Hambye and B. Zaldivar, *Production regimes for self-interacting dark matter*, *JCAP* **03** (2016) 018 [arXiv:1510.08063] [ɪɴSPIRE].

[20] K.K. Boddy, M. Kaplinghat, A. Kwa and A.H.G. Peter, *Hidden sector hydrogen as dark matter: small-scale structure formation predictions and the importance of hyperfine interactions*, *Phys. Rev.* **D 94** (2016) 123017 [arXiv:1609.03592] [ɪɴSPIRE].

[21] T. Bringmann, H.T. Ihle, J. Kersten and P. Walia, *Suppressing structure formation at dwarf galaxy scales and below: late kinetic decoupling as a compelling alternative to warm dark matter*, *Phys. Rev.* **D 94** (2016) 103529 [arXiv:1603.04884] [ɪɴSPIRE].

[22] T. Binder, M. Gustafsson, A. Kamada, S.M.R. Sandner and M. Wiesner, *Reannihilation of self-interacting dark matter*, *Phys. Rev.* **D 97** (2018) 123004 [arXiv:1712.01246] [ɪɴSPIRE].

[23] E. Ma, *Inception of self-interacting dark matter with dark charge conjugation symmetry*, *Phys. Lett.* **B 772** (2017) 442 [arXiv:1704.04666] [ɪɴSPIRE].

[24] R. Huo, M. Kaplinghat, Z. Pan and H.-B. Yu, *Signatures of self-interacting dark matter in the matter power spectrum and the CMB*, arXiv:1709.09717 [ɪɴSPIRE].

[25] I. Baldes, M. Cirelli, P. Panci, K. Petraki, F. Sala and M. Taoso, *Asymmetric dark matter: residual annihilations and self-interactions*, arXiv:1712.07489 [ɪɴSPIRE].

[26] T. Bringmann, F. Kahlhoefer, K. Schmidt-Hoberg and P. Walia, *Converting non-relativistic dark matter to radiation*, arXiv:1803.03644 [ɪɴSPIRE].

[27] B. Zhu, R. Ding and Y. Li, *Realization of sneutrino self-interacting dark matter in the focus point supersymmetry*, arXiv:1804.00277 [ɪɴSPIRE].

[28] M. Duerr, K. Schmidt-Hoberg and S. Wild, *Self-interacting dark matter with a stable vector mediator*, arXiv:1804.10385 [ɪɴSPIRE].

[29] M. Kaplinghat, T. Linden and H.-B. Yu, *Galactic center excess in γ rays from annihilation of self-interacting dark matter*, *Phys. Rev. Lett.* **114** (2015) 211303 [arXiv:1501.03507] [ɪɴSPIRE].

[30] T. Bringmann, F. Kahlhoefer, K. Schmidt-Hoberg and P. Walia, *Strong constraints on self-interacting dark matter with light mediators*, *Phys. Rev. Lett.* **118** (2017) 141802 [arXiv:1612.00845] [ɪɴSPIRE].

[31] Muon G-2 collaboration, G.W. Bennett et al., *Final report of the E821 muon anomalous magnetic moment measurement at BNL*, *Phys. Rev.* **D 73** (2006) 072003 [hep-ex/0602035] [ɪɴSPIRE].

[32] B.L. Roberts, *Status of the Fermilab muon $(g-2)$ experiment*, *Chin. Phys.* **C 34** (2010) 741 [arXiv:1001.2898] [ɪɴSPIRE].

[33] J. Prades, E. de Rafael and A. Vainshtein, *The hadronic light-by-light scattering contribution to the muon and electron anomalous magnetic moments*, *Adv. Ser. Direct. High Energy Phys.* **20** (2009) 303 [arXiv:0901.0306] [INSPIRE].

[34] F. Jegerlehner and A. Nyffeler, *The muon g − 2*, *Phys. Rept.* **477** (2009) 1 [arXiv:0902.3360] [INSPIRE].

[35] S. Baek, N.G. Deshpande, X.-G. He and P. Ko, *Muon anomalous g − 2 and gauged L_μ-L_τ models*, *Phys. Rev.* **D 64** (2001) 055006 [hep-ph/0104141] [INSPIRE].

[36] J. Heeck and W. Rodejohann, *Gauged L_μ-L_τ symmetry at the electroweak scale*, *Phys. Rev.* **D 84** (2011) 075007 [arXiv:1107.5238] [INSPIRE].

[37] K.R. Lynch, *Extended electroweak interactions and the muon g_μ − 2*, *Phys. Rev.* **D 65** (2002) 053006 [hep-ph/0108080] [INSPIRE].

[38] PLANCK collaboration, P.A.R. Ade et al., *Planck 2015 results. XIII. Cosmological parameters*, *Astron. Astrophys.* **594** (2016) A13 [arXiv:1502.01589] [INSPIRE].

[39] CHARM-II collaboration, D. Geiregat et al., *First observation of neutrino trident production*, *Phys. Lett.* **B 245** (1990) 271 [INSPIRE].

[40] S.R. Mishra et al., *Neutrino tridents and W-Z interference*, *Phys. Rev. Lett.* **66** (1991) 3117 [INSPIRE].

[41] W. Altmannshofer, S. Gori, M. Pospelov and I. Yavin, *Neutrino trident production: a powerful probe of new physics with neutrino beams*, *Phys. Rev. Lett.* **113** (2014) 091801 [arXiv:1406.2332] [INSPIRE].

[42] BaBar collaboration, J.P. Lees et al., *Search for a muonic dark force at BABAR*, *Phys. Rev.* **D 94** (2016) 011102 [arXiv:1606.03501] [INSPIRE].

[43] BOREXINO collaboration, G. Bellini et al., *Precision measurement of the ^7Be solar neutrino interaction rate in Borexino*, *Phys. Rev. Lett.* **107** (2011) 141302 [arXiv:1104.1816] [INSPIRE].

[44] M. Bauer, P. Foldenauer and J. Jaeckel, *Hunting all the hidden photons*, arXiv:1803.05466 [INSPIRE].

[45] H.K. Dreiner, J.-F. Fortin, J. Isern and L. Ubaldi, *White dwarfs constrain dark forces*, *Phys. Rev.* **D 88** (2013) 043517 [arXiv:1303.7232] [INSPIRE].

[46] R. Harnik, J. Kopp and P.A.N. Machado, *Exploring ν signals in dark matter detectors*, *JCAP* **07** (2012) 026 [arXiv:1202.6073] [INSPIRE].

[47] NA48/2 collaboration, J.R. Batley et al., *Search for the dark photon in π^0 decays*, *Phys. Lett.* **B 746** (2015) 178 [arXiv:1504.00607] [INSPIRE].

[48] A. Kamada and H.-B. Yu, *Coherent propagation of PeV neutrinos and the dip in the neutrino spectrum at IceCube*, *Phys. Rev.* **D 92** (2015) 113004 [arXiv:1504.00711] [INSPIRE].

[49] T. Asaka and M. Kawasaki, *Cosmological moduli problem and thermal inflation models*, *Phys. Rev.* **D 60** (1999) 123509 [hep-ph/9905467] [INSPIRE].

[50] D.J. Fixsen, E.S. Cheng, J.M. Gales, J.C. Mather, R.A. Shafer and E.L. Wright, *The cosmic microwave background spectrum from the full COBE FIRAS data set*, *Astrophys. J.* **473** (1996) 576 [astro-ph/9605054] [INSPIRE].

[51] M. Kawasaki, K. Kohri, T. Moroi and Y. Takaesu, *Revisiting big-bang nucleosynthesis constraints on long-lived decaying particles*, *Phys. Rev.* **D 97** (2018) 023502 [arXiv:1709.01211] [INSPIRE].

[52] K. Griest and D. Seckel, *Three exceptions in the calculation of relic abundances*, *Phys. Rev.* **D 43** (1991) 3191 [INSPIRE].

[53] J. Hisano, S. Matsumoto, M. Nagai, O. Saito and M. Senami, *Non-perturbative effect on thermal relic abundance of dark matter*, *Phys. Lett.* **B 646** (2007) 34 [hep-ph/0610249] [INSPIRE].

[54] J.L. Feng, M. Kaplinghat and H.-B. Yu, *Sommerfeld enhancements for thermal relic dark matter*, *Phys. Rev.* **D 82** (2010) 083525 [arXiv:1005.4678] [INSPIRE].

[55] S. Tulin, H.-B. Yu and K.M. Zurek, *Beyond collisionless dark matter: particle physics dynamics for dark matter halo structure*, *Phys. Rev.* **D 87** (2013) 115007 [arXiv:1302.3898] [INSPIRE].

[56] F. Kahlhoefer, K. Schmidt-Hoberg and S. Wild, *Dark matter self-interactions from a general spin-0 mediator*, *JCAP* **08** (2017) 003 [arXiv:1704.02149] [INSPIRE].

[57] F. Kahlhoefer, K. Schmidt-Hoberg, M.T. Frandsen and S. Sarkar, *Colliding clusters and dark matter self-interactions*, *Mon. Not. Roy. Astron. Soc.* **437** (2014) 2865 [arXiv:1308.3419] [INSPIRE].

[58] A.B. Newman, T. Treu, R.S. Ellis and D.J. Sand, *The density profiles of massive, relaxed galaxy clusters: II. Separating luminous and dark matter in cluster cores*, *Astrophys. J.* **765** (2013) 25 [arXiv:1209.1392] [INSPIRE].

[59] S. Tulin, H.-B. Yu and K.M. Zurek, *Resonant dark forces and small-scale structure*, *Phys. Rev. Lett.* **110** (2013) 111301 [arXiv:1210.0900] [INSPIRE].

[60] PANDAX-II collaboration, X. Ren et al., *Particle physics constraints on self-interacting dark matter from PandaX-II experiment*, arXiv:1802.06912 [INSPIRE].

[61] SUPER-KAMIOKANDE collaboration, K. Frankiewicz, *Searching for dark matter annihilation into neutrinos with Super-Kamiokande*, in *Proceedings, Meeting of the APS Division of Particles and Fields (DPF 2015)*, Ann Arbor, MI, U.S.A., 4–8 August 2015 [arXiv:1510.07999] [INSPIRE].

[62] LUX collaboration, D.S. Akerib et al., *First results from the LUX dark matter experiment at the Sanford Underground Research Facility*, *Phys. Rev. Lett.* **112** (2014) 091303 [arXiv:1310.8214] [INSPIRE].

[63] F. D'Eramo, B.J. Kavanagh and P. Panci, *You can hide but you have to run: direct detection with vector mediators*, *JHEP* **08** (2016) 111 [arXiv:1605.04917] [INSPIRE].

[64] ICECUBE collaboration, M.G. Aartsen et al., *Observation of high-energy astrophysical neutrinos in three years of IceCube data*, *Phys. Rev. Lett.* **113** (2014) 101101 [arXiv:1405.5303] [INSPIRE].

[65] ICECUBE collaboration, M.G. Aartsen et al., *The IceCube neutrino observatory — contributions to ICRC 2017 Part II: properties of the atmospheric and astrophysical neutrino flux*, arXiv:1710.01191 [INSPIRE].

[66] T. Araki, F. Kaneko, Y. Konishi, T. Ota, J. Sato and T. Shimomura, *Cosmic neutrino spectrum and the muon anomalous magnetic moment in the gauged L_μ-L_τ model*, *Phys. Rev.* **D 91** (2015) 037301 [arXiv:1409.4180] [INSPIRE].

[67] T. Araki, F. Kaneko, T. Ota, J. Sato and T. Shimomura, *MeV scale leptonic force for cosmic neutrino spectrum and muon anomalous magnetic moment*, *Phys. Rev.* **D 93** (2016) 013014 [arXiv:1508.07471] [INSPIRE].

[68] M. Ibe, W. Nakano and M. Suzuki, *Constraints on L_μ-L_τ gauge interactions from rare kaon decay*, *Phys. Rev.* **D 95** (2017) 055022 [arXiv:1611.08460] [INSPIRE].

[69] Y. Kaneta and T. Shimomura, *On the possibility of a search for the L_μ-L_τ gauge boson at Belle-II and neutrino beam experiments*, *PTEP* **2017** (2017) 053B04 [arXiv:1701.00156] [INSPIRE].

[70] S.N. Gninenko and N.V. Krasnikov, *Probing the muon $g_\mu - 2$ anomaly, L_μ-L_τ gauge boson and dark matter in dark photon experiments*, arXiv:1801.10448 [INSPIRE].

[71] M. Abdullah, J.B. Dent, B. Dutta, G.L. Kane, S. Liao and L.E. Strigari, *Coherent Elastic Neutrino Nucleus Scattering (CEνNS) as a probe of Z' through kinetic and mass mixing effects*, arXiv:1803.01224 [INSPIRE].

[72] Y. Kahn, G. Krnjaic, N. Tran and A. Whitbeck, *M^3: a new muon missing momentum experiment to probe $(g-2)_\mu$ and dark matter at Fermilab*, arXiv:1804.03144 [INSPIRE].

[73] K. Asai, K. Hamaguchi and N. Nagata, *Predictions for the neutrino parameters in the minimal gauged* $U(1)_{L_\mu - L_\tau}$ *model*, *Eur. Phys. J.* **C 77** (2017) 763 [arXiv:1705.00419] [INSPIRE].

[74] S. Bilmis, I. Turan, T.M. Aliev, M. Deniz, L. Singh and H.T. Wong, *Constraints on dark photon from neutrino-electron scattering experiments*, *Phys. Rev.* **D 92** (2015) 033009 [arXiv:1502.07763] [INSPIRE].

[75] Y.S. Jeong, C.S. Kim and H.-S. Lee, *Constraints on the* $U(1)_L$ *gauge boson in a wide mass range*, *Int. J. Mod. Phys.* **A 31** (2016) 1650059 [arXiv:1512.03179] [INSPIRE].